



## Single-cell Rapid Capture Hybridization sequencing reliably detects isoform usage and coding mutations in targeted genes

Hongke Peng, Jafar S. Jabbari, Luyi Tian, et al.

*Genome Res.* 2025 35: 942-955 originally published online January 10, 2025

Access the most recent version at doi:[10.1101/gr.279322.124](https://doi.org/10.1101/gr.279322.124)

---

**References** This article cites 36 articles, 2 of which can be accessed free at:  
<http://genome.cshlp.org/content/35/4/942.full.html#ref-list-1>

**Open Access** Freely available online through the *Genome Research* Open Access option.

**Creative Commons License** This article, published in *Genome Research*, is available under a Creative Commons License (Attribution-NonCommercial 4.0 International), as described at <http://creativecommons.org/licenses/by-nc/4.0/>.

**Email Alerting Service** Receive free email alerts when new articles cite this article - sign up in the box at the top right corner of the article or [click here](#).



---

To subscribe to *Genome Research* go to:  
<https://genome.cshlp.org/subscriptions>

## Method

# Single-cell Rapid Capture Hybridization sequencing reliably detects isoform usage and coding mutations in targeted genes

Hongke Peng,<sup>1,2</sup> Jafar S. Jabbari,<sup>1,2</sup> Luyi Tian,<sup>1,2,9</sup> Changqing Wang,<sup>1,2</sup> Yupei You,<sup>1,2</sup> Chong Chyn Chua,<sup>1,2,3,4</sup> Natasha S. Anstee,<sup>1,2</sup> Noorul Amin,<sup>1,2</sup> Andrew H. Wei,<sup>1,2,5</sup> Nadia M. Davidson,<sup>1,2</sup> Andrew W. Roberts,<sup>1,2,5</sup> David C.S. Huang,<sup>1,2</sup> Matthew E. Ritchie,<sup>1,2,8</sup> and Rachel Thijssen<sup>1,2,6,7,8</sup>

<sup>1</sup>The Walter and Eliza Hall Institute of Medical Research, Melbourne 3052, Australia; <sup>2</sup>Department of Medical Biology, University of Melbourne, Melbourne 3052, Australia; <sup>3</sup>Monash Haematology, Monash Health, Melbourne 3168, Australia; <sup>4</sup>Clinical Haematology, Northern Health, Melbourne 3076, Australia; <sup>5</sup>Department of Clinical Haematology, Royal Melbourne Hospital and Peter MacCallum Cancer Centre, Melbourne 3052, Australia; <sup>6</sup>Department of Hematology, Amsterdam UMC, Amsterdam 1081HV, the Netherlands; <sup>7</sup>Cancer Center Amsterdam, Cancer Biology and Immunology, Amsterdam 1081HV, the Netherlands

Single-cell long-read sequencing has transformed our understanding of isoform usage and the mutation heterogeneity between cells. Despite unbiased in-depth analysis, the low sequencing throughput often results in insufficient read coverage, thereby limiting our ability to perform mutation calling for specific genes. Here, we developed a single-cell Rapid Capture Hybridization sequencing (scRaCH-seq) method that demonstrates high specificity and efficiency in capturing targeted transcripts using long-read sequencing, allowing an in-depth analysis of mutation status and transcript usage for genes of interest. The method includes creating a probe panel for transcript capture, using barcoded primers for pooling and efficient sequencing via Oxford Nanopore Technologies platforms. scRaCH-seq is applicable to stored and indexed single-cell cDNA, which allows analysis to be combined with existing short-read RNA-seq data sets. In our investigation of *BTK* and *SF3B1* genes in samples from patients with chronic lymphocytic leukemia (CLL), we detect *SF3B1* isoforms and mutations with high sensitivity. Integration with short-read single-cell RNA sequencing (scRNA-seq) data reveals significant gene expression differences in *SF3B1*-mutated CLL cells, although it does not impact the sensitivity of the anticancer drug venetoclax. scRaCH-seq's capability to study long-read transcripts of multiple genes makes it a powerful tool for single-cell genomics.

[Supplemental material is available for this article.]

Single-cell sequencing technologies have revolutionized our understanding of cell state and function (Tang et al. 2009; Sandberg 2014). These approaches enable the comprehensive characterization of individual cells, revealing cancer biology and tumor heterogeneity (Stewart et al. 2020; Wang et al. 2020, 2022; Liu et al. 2022; Mustachio and Roszik 2022; Tian et al. 2022; Nagler and Wu 2023). While single-cell RNA sequencing (scRNA-seq) has been widely used for transcriptomic profiling of individual cells, it has limitations in calling mutations and quantifying isoform usage due to the 5' and 3' bias induced by the fragmentation step in the library preparation protocol and the widespread use of short-read technology for sequencing samples. Consequently, linking the single-cell transcriptome to the mutation status of cancer cells becomes a challenge. Understanding the clonal and nonclonal mechanisms of selection and adaptation in response to therapeutic pressure is of importance. Moreover, the influence of isoform usage on cell states further underscores the need for comprehensive methodologies. In response to these challenges, alternative methods have

emerged to link the transcriptome profile to isoform usage, mutations, and translocations in full-length transcripts at a single-cell level (Wu and Schmitz 2023).

In recent years, several high-throughput methods have been developed to enable single-cell long-read sequencing. These approaches typically involve barcoding of cDNA using existing methods such as 10x Genomics or Drop-seq and sequencing the indexed full-length cDNA on platforms such as Pacific Biosciences (PacBio) or Oxford Nanopore Technologies (ONT) (Lebrigand et al. 2020; Joglekar et al. 2023). While these unbiased single-cell long-read sequencing methods can detect a larger number of isoforms at a single-cell level, the lower overall sequencing level per cell reduces the ability to accurately quantify isoform usage and mutation calling. To overcome this challenge, other methods were developed to target genes of interest, but these methods often require primer spike-in with the 10x Genomics protocol and primer panel design optimization (Nam et al. 2019; Griffin et al. 2023). This limits the ability to target multiple genes of interest or to perform long-read sequencing on already amplified single-cell indexed cDNA.

<sup>8</sup>Joint senior authors.

<sup>9</sup>Present address: Guangzhou Laboratory, Guangdong 510005, China  
Corresponding author: [r.thijssen@amsterdamumc.nl](mailto:r.thijssen@amsterdamumc.nl)

Article published online before print. Article, supplemental material, and publication date are at <https://www.genome.org/cgi/doi/10.1101/gr.279322.124>. Freely available online through the *Genome Research* Open Access option.

© 2025 Peng et al. This article, published in *Genome Research*, is available under a Creative Commons License (Attribution-NonCommercial 4.0 International), as described at <http://creativecommons.org/licenses/by-nc/4.0/>.

The growing interest in high-throughput single-cell multiomic methods to enhance our understanding of cancer complexity led us to develop a method that can flexibly link genotypes in single cells to preexisting short-read transcriptome data generated by various 10x Genomics protocols. CITE-seq combines transcriptome with cell surface protein expression and 10x Genomics multiome combines transcriptome with chromatin accessibility data (Stoeckius et al. 2017). Our single-cell Rapid Capture Hybridization sequencing (scRaCH-seq) method enables the capture of multiple transcripts from preindexed and stored cDNA independent of the 10x Genomics kit used. This approach uses biotinylated probes to target genes of interest and Streptavidin beads for on-target transcript enrichment. It was first detailed in Thijssen et al. (2022), to capture the transcriptional landscape of 17 *BCL2* family genes in patients with chronic lymphocytic leukemia (CLL). That study investigated the resistance mechanisms observed in CLL cells after treatment with the *BCL2* inhibitor venetoclax treatment. Using scRaCH-seq, we successfully identified the *BCL2* G101V mutation, a novel *PMAIP1* transcript, and a unique *BAX* isoform across different venetoclax-relapsed samples at a single-cell level. Despite the first application of scRaCH-seq to that research, a detailed method description, data analysis, and method evaluation have not been published.

Here, we provide a comprehensive description of the scRaCH-seq method in which we target the transcripts of 2 genes *SF3B1* and *BTK* as illustrative examples. The aim of this study is to demonstrate the utility and accuracy of scRaCH-seq in detecting gene-specific mutations and splicing events in single cells, with a focus on probe-capture efficiency, artifact diagnostics, and mutation/deletion calling.

## Results

### Assessing data quality and probe-capture efficiency

A step-by-step guide to probe panel design (Supplemental Fig. S1) was created to facilitate the application of scRaCH-seq together with a tailored analysis pipeline that extends the *FLAMES* (Full-Length Analysis of Mutations and Splicing) R package (Tian et al. 2021) and incorporates additional read integrity checks and steps to remove background noise. After scRaCH-seq was performed (Fig. 1), a total of 43,762,097 raw reads were acquired through Nanopore sequencing across 21 samples, with a read length distribution spanning from 0 to 4000 bp (Fig. 2A). The *FLAMES* demultiplexing process was subsequently able to recover 28,573,271 reads that could be attributed to specific cells. Despite an overall 35% read loss during this step, the length distribution of the retained reads remained unaltered (Fig. 2A). After demultiplexing, sufficient reads (~1,000,000) were preserved for each sample (Fig. 2B). We also tested Flexiplex (Cheng et al. 2024) and the reads retained for downstream processing were similar. Next demultiplexed reads without template switch oligo (TSO) sequences and poly(A) tails were discarded following the quality control step which eliminated ~49% of reads, primarily those with lengths <1500 bp (Fig. 2A). A total of 14,442,490 reads were retained for subsequent read alignment and feature counting. Despite some read loss during demultiplexing and read integrity checks, we achieved an average saturation rate exceeding 75% for the target genes across all samples (Supplemental Fig. S2A,B). Additionally, there was an increase in unique molecular identifiers (UMIs) as more transcripts were sequenced for each sample (Supplemental Fig. S2C,D). scRaCH-seq exhibited lower read loss during both

demultiplexing and read integrity checks compared to single-cell full-length transcript sequencing (scFLT-seq), an unbiased single-cell long-read sequencing method (Supplemental Fig. S2E–G).

scRaCH-seq and our *FLAMES* pipeline effectively captured the majority of cell barcodes identified by Cell Ranger in scRNA-seq data (Fig. 2B). After quality control, 92.6% of all the reads retained aligned successfully to the targeted genes *SF3B1* and *BTK* (Fig. 2B; Supplemental Fig. S3A). Duplicated reads were collapsed based on isoforms. In concordance with on-target reads, a high number of UMIs were associated with *SF3B1* and *BTK*, with the majority of captured cells harboring the target genes (Fig. 2C). Most of the off-target UMIs arose from single reads (Supplemental Fig. S3B), indicating the presence of low levels of background signal in the data. The captured off-target genes include *HSPD1*, which is near *SF3B1*, and *TIMM8A*, located in close proximity to the *BTK* gene (Fig. 2D). These were likely read-through transcripts. Additionally, some other top off-target transcripts, such as *RPL13*, were captured due to shared sequences with the target transcripts (Supplemental Fig. S3C). However, another group of off-target transcripts, such as *CD74*, were neither located near the target genes nor shared similar sequences with them. This type of off-target transcript is likely attributable to sequencing background. Per-cell UMI counts for the target genes in the corresponding short-read data were evaluated, revealing a higher per-cell UMI capture in the scRaCH-seq data for *SF3B1* and *BTK* (Fig. 2E). In a separate scRaCH-seq experiment targeting 17 *BCL2* family genes in CLL cells, similar UMI counts were observed in scRaCH-seq data compared to short-read data (Supplemental Fig. S4A). In another experiment using acute myeloid leukemia (AML) cells with similar read length distribution as the CLL samples (Fig. 2A; Supplemental Fig. S4B), we successfully captured the transcripts of 24 genes (Supplemental Fig. S4C). The AML sample was processed using the 10x Genomics Chromium single-cell 3' kit. These findings indicate the high efficiency of scRaCH-seq in capturing the transcripts of target genes observed in matched single-cell 5' and 3' short-read data sets via long-read sequencing.

Next, we compared the gene expression of *SF3B1* and *BTK* in the scRaCH-seq data with the short-read data set. Similar to the short-read gene expression data, scRaCH-seq showed that *BTK* expression was detected in the CLL/B cell population, whereas *SF3B1* was expressed across all cell types (Fig. 2F–H)

### Isoform detection by scRaCH-seq

Given that scRaCH-seq operates by capturing transcripts of target genes with probes, it enables the exploration of isoform usage for the targeted genes. In our data set, we incorporated the CLL and B cells from matched samples from CLL patients at diagnosis, after venetoclax relapse, in patients who relapsed and subsequently received a BTK inhibitor (BTKi) and healthy donor (HD) samples (Thijssen et al. 2022). The primary *BTK* isoform (*BTK-201*, ENST00000308731) captured by scRaCH-seq is a protein-coding isoform with 19 exons, exhibiting high expression across all samples (Fig. 3A). The other four transcripts among the top 5 captured isoforms by scRaCH-seq are novel isoforms not cataloged previously (Fig. 3A). Transcripts #2 and #3 lack the last four exons compared to *BTK-201*, with transcript #2 having a 16 bp longer exon 10 compared to transcript #3. Novel transcript #4 lacks exon 10 compared to the *BTK-201* transcripts. While all five *BTK* transcripts detected by scRaCH-seq have a poly(A) tail in the 3' UTR, transcript #5, comprising only three exons, has a different starting point at the 5' UTR. Consequently, it remains uncertain whether

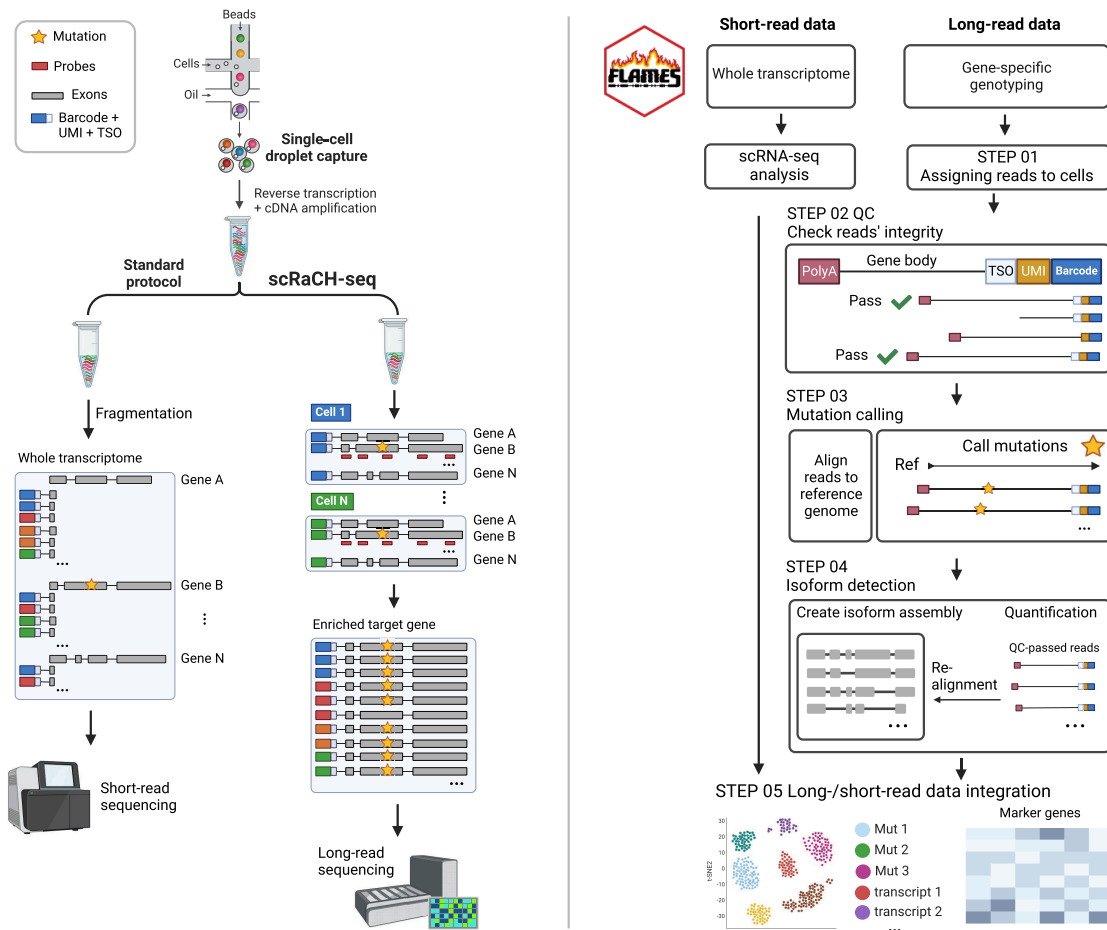


**Figure 1.** Schematic of scRaCH-seq approach and *FLAMES* pipeline for single-cell long-read data analysis. scRaCH-seq can be incorporated in the standard high-throughput single-cell RNA-seq experiments (left side). After single-cell isolation, mRNA is converted into cDNA and barcoded. Only some of this amplified indexed cDNA is used for short-read library preparation and Illumina sequencing. The surplus cDNA is stored and can be used for scRaCH-seq. For scRaCH-seq, a probe panel is designed for genes of interest. The biotinylated probes are hybridized with amplified cDNA overnight. The probes and target genes are captured with Streptavidin beads, washed, and amplified. The enriched target long-read transcripts are sequenced on the Nanopore platform. With the *FLAMES* pipeline, FASTQ files are demultiplexed by cross-referencing the cell barcodes identified in scRNA-seq data (STEP 01). Next, the demultiplexed reads undergo an integrity check and the reads that possess a UMI, a TSO sequence, and poly(A) tails are retained (STEP 02). Reads are aligned to the GRCh38 reference genome to construct a transcript assembly. Concurrently, the piled-up reads are compared against GRCh38 to identify base alterations and deletions, generating a comprehensive mutation/deletion matrix (STEP 03). The reads are realigned to the transcript assembly for quantification (STEP 04). Single-cell short-read gene expression data is used to cluster the cells, based on the conventional analysis pipeline for scRNA-seq. The transcript usage and mutation/deletion information are then aligned with the single-cell gene expression data. The bridge connecting these data sets is the shared cell barcodes, ensuring the gene expression profile at a transcript level (STEP 05).

*BTK* transcript #5 is an artifact resulting from truncation at the 5' end. No evidence of differential *BTK* transcript usage was found across the different sample groups (Fig. 3A). Among the *BTK* transcripts, four of them shared a nearby TSS with the primary *BTK* isoform, except for *BTK* transcript #5 (Fig. 3A). However, *BTK* transcript #5 also shared a nearby TSS with another annotated isoform (Supplemental Fig. S5A). Additionally, TSS signals were detected in this region in the CAGE database (FANTOM6) (Supplemental Fig. S5B).

In our investigation of the *SF3B1* isoforms, a previously unidentified *SF3B1* transcript emerged as the predominant form, characterized by the absence of the last 14 exons in the 3' end (Fig. 3B). Given that this transcript is not the canonical *SF3B1* transcript expressed in the majority of cells, including HD samples, we undertook a comprehensive assessment to determine its authenticity. This transcript does not appear to be an artifact induced by Nanopore sequencing, since it initiates at exon 1 and concludes

with a poly(A) tail. To further validate its presence, we examined the distribution of *SF3B1* reads in scRaCH-seq data and compared it to matched bulk RNA-seq and scFLT-seq data for sample CLL2-RB. A consistent pattern in the *SF3B1* read distribution between scRaCH-seq and scFLT-seq was observed, with a higher coverage of exons 1–11 compared to that of exons 12–25 (Supplemental Fig. S6A). However, when comparing single-cell sequencing data (scRaCH-seq and scFLT-seq) to bulk RNA-seq, bulk RNA-seq data exhibited a relatively stable read coverage across all exons (Supplemental Fig. S6B). This hints at a potential bias introduced by the 10x Genomics protocol into the composition of *SF3B1* transcripts. Upon closer examination, we discovered that 86% of single-cell reads mapped to exon 11 contained three cytosine (C) to thymine (T) mismatches following the drop in read coverage, indicating that these reads were created due to the unexpected binding of 10x poly(A) primers (Supplemental Fig. S6C). This artifact is reflected in the read length distribution plot with a higher

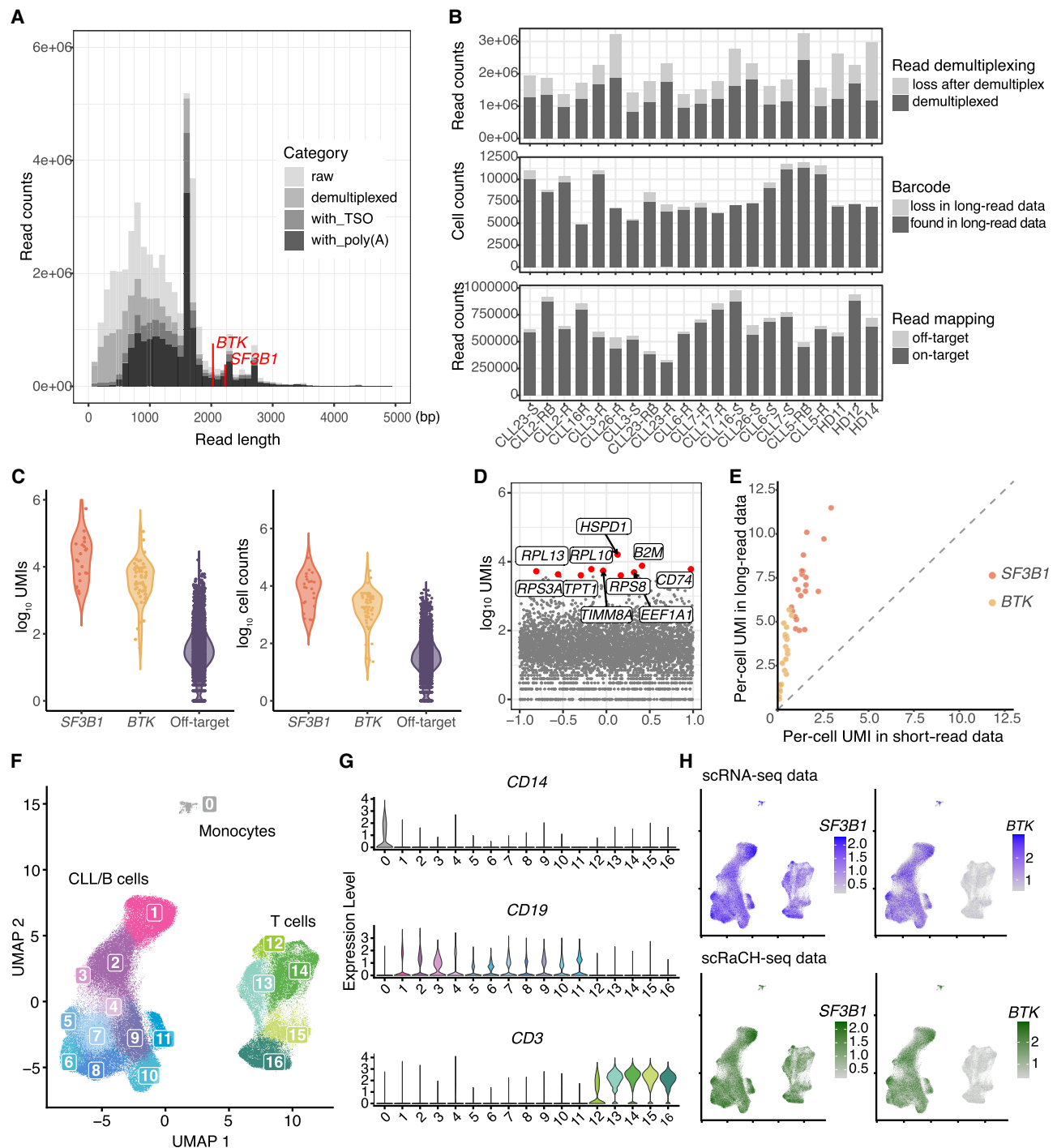


**Figure 2.** scRaCH-seq is efficient in capturing enriched genes of interest. (A) A graph showing the losses in read counts due to demultiplexing and integrity checks, depicting the distribution of read lengths ranging from 0 to 5000 bp. The canonical isoform of *BTK* (2027 bp) and *SF3B1* (2225 bp) are marked on the plot. The four shades of gray, ranging from light to dark, correspond to raw reads, demultiplexed reads, reads with TSO, and reads with also a poly(A) end. (B) Bar plots showing the loss of reads after demultiplexing (top panel), barcodes detected in long-read sequencing data (middle panel), and counts of off-target and on-target reads for each sample (bottom panel). (C) Violin plot showing the  $\log_{10}$  UMI counts of collapsed *BTK* (red), *SF3B1* (orange), and off-target transcripts (purple) based on isoform detected by scRaCH-seq (left panel). Violin plot showing the  $\log_{10}$  counts of cells possessing collapsed transcripts of *BTK* (red), *SF3B1* (orange), and off-target genes (purple) (right panel). (D) Dot plot showing the  $\log_{10}$  counts of off-target genes with the top 10 off-target transcripts specifically marked. (E) Dot plot showing the per-cell UMIs of *SF3B1* (red) and *BTK* (orange), detected by scRNA-seq (x-axis) and scRaCH-seq (y-axis) for all samples. (F) Uniform Manifold Approximation and Projection (UMAP) projection of peripheral blood mononuclear cells from CLL patients or healthy donors and clustering based on short-read gene expression. (G) Violin plot showing the expression of *CD14* (monocyte marker), *CD19* (B/CLL cell marker), and *CD3* (T cell marker) per cell cluster (F). (H) UMAP projection of *SF3B1* (left) and *BTK* (right) gene-level expression detected by scRNA-seq (purple) or scRaCH-seq (green).

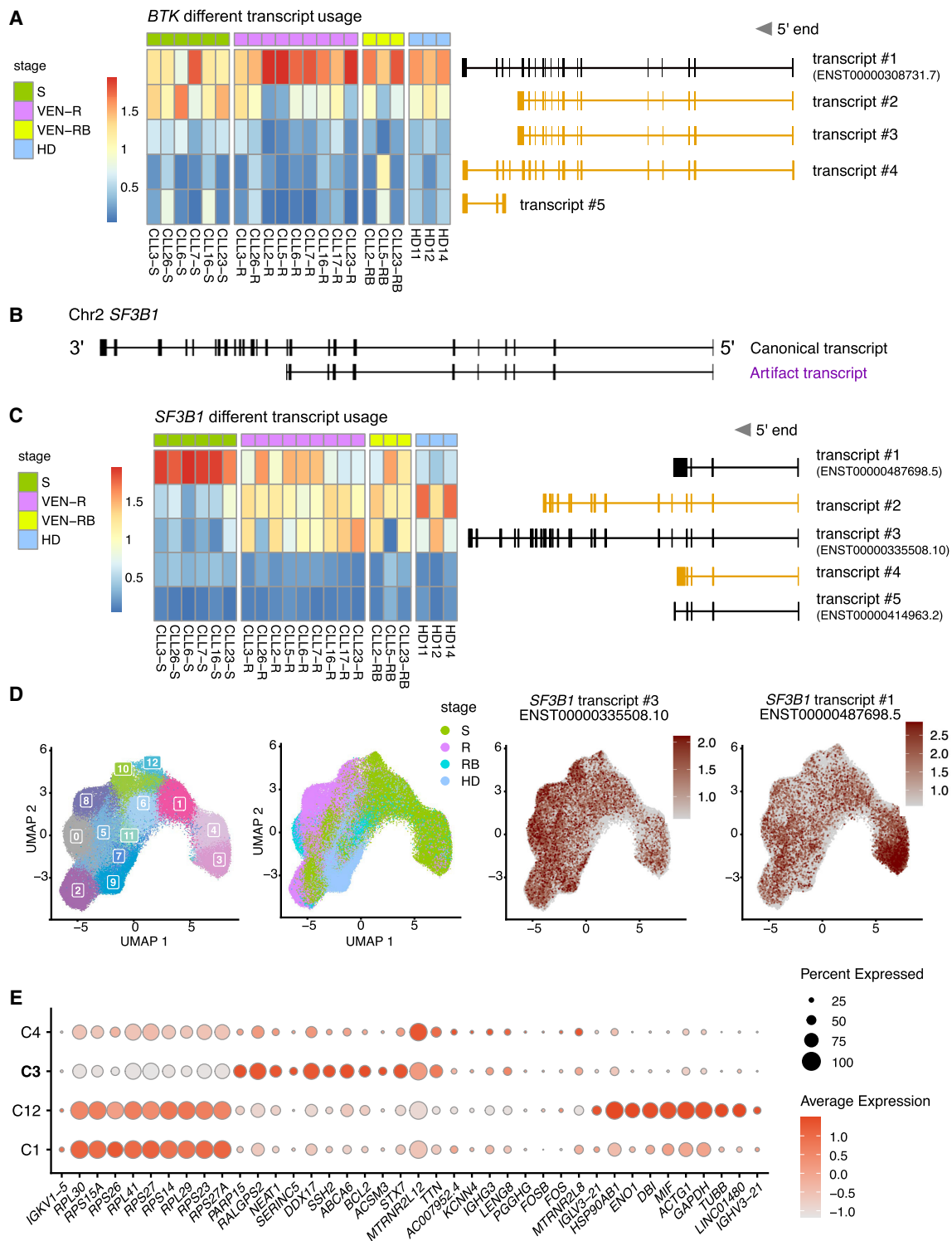


**Figure 3.** scRaCH-seq reveals different *SF3B1* isoform usage by CLL cells from patients undergoing different treatments. (A) Heatmap showing *BTK* isoform usage (rows) per sample (columns) in the B/CLL cells. The top 5 *BTK* transcripts are illustrated on the right with novel transcripts highlighted in yellow. Samples are grouped in screening (S; green), venetoclax-relapsed (VEN-R/R; pink), venetoclax-relapsed and subsequently on BTKi (VEN-RB/RB; bright yellow), and HD (turquoise). (B) Illustration of the dominant *SF3B1* transcript identified and characterized by the absence of the last 14 exons in the 3' end (highlighted in purple). (C) Heatmap showing *SF3B1* isoform usage (rows) per sample (columns) in the B/CLL cells. The top 5 *SF3B1* transcripts are illustrated on the right with novel transcripts highlighted in yellow. (D) UMAP projection of CLL/B cells from CLL patients or HDs and clustering based on short-read gene expression. The samples from CLL patients at screening (S; green), venetoclax-relapsed (R; pink), venetoclax-relapsed and subsequently on BTKi (RB; bright yellow) and HDs (turquoise) are highlighted in the UMAP. The expression of the *SF3B1* transcripts #1 and #3 is overlaid as red dots in the UMAP (B). (E) Dot plot showing marker genes that distinguish the CLL cells present in the four clusters shared by the screening samples (C1, C3, C4, and C12 in C). Cluster 3 with *SF3B1* transcript #1 usage is indicated in bold.

proportion of reads shorter than the canonical isoforms of *SF3B1* (Fig. 2A). These artifacts were subsequently removed from the scRaCH-seq data, resulting in the elimination of the novel *SF3B1* transcript which lacks the last 14 exons (Supplemental Fig. S6D).

After removal of the artifacts, high expression levels of *SF3B1* transcript #1 (*SF3B1-211*, ENST00000487698), transcript #2 (a novel transcript containing exons 1–16), and transcript #3 (*SF3B1-201*, ENST00000335508) were consistently observed across multiple samples (Fig. 3C). The expression of transcripts #4 (a novel transcript) and #5 (*SF3B1-204*, ENST00000414963) was relatively low (Fig. 3C). In contrast to *BTK*, a clear difference in *SF3B1* isoform usage was evident between CLL cells from patient samples at screening and those from other CLL stages or HD B cells (Fig. 3C). Specifically, *SF3B1* transcript #1 was highly expressed in screening samples, whereas transcripts #2 and #3 were highly expressed in venetoclax-relapsed and HD samples. In contrast to the CLL and B cells, *SF3B1* transcript #3 was the dominant transcript expressed by the T cells from the CLL patients at different stages and HDs (Supplemental Fig. S7). To investigate why the screening samples exhibit higher expression of transcript #1, we linked isoform usage with gene expression. The CLL and B cells from all samples were isolated and reclustered, revealing distinct clusters of the different stages, including one B cell cluster (C9), four screening clusters (C1, C3, C4, and C12), three relapsed clusters (C0, C2, and C8), and five clusters shared by screening and relapsed CLL cells (C5, C6, C7, C10, and C11) (Fig. 3D). *SF3B1* transcript #1 was specific to the screening CLL cells from cluster 3 (Fig. 3D). Meanwhile, transcript #3, the canonical *SF3B1* isoform, was expressed by all CLL and B cells (Fig. 3D). Subsequently, single-cell differential gene expression analysis between all the screening clusters (C1, C3, C4, and C12) was performed. For this analysis, other clusters were excluded to eliminate confounding factors related to treatment stages. CLL cells in C3 exhibited a high expression level of *DDX17*, a gene involved in almost all RNA metabolism processes (Xu et al. 2023), and *PARP15*, a negative regulator of transcription (Fig. 3E; Ryu et al. 2015).

### Calling *SF3B1* mutations using scRaCH-seq data

Besides isoform detection, scRaCH-seq has the ability of linking the mutation status to cell state and differential gene expression. Among the CLL patients treated with venetoclax, *SF3B1* mutation was detected in five samples by whole exome sequencing (WES) (Thijssen et al. 2022) which was used as a ground truth to validate the scRaCH-seq data. For the identification of *SF3B1* mutations, we aggregated the scRaCH-seq data from all the samples, revealing many *SF3B1* transcripts with single-nucleotide polymorphism (SNP) (Fig. 4A). The three most prominent SNPs were #5, #6, and #8. While SNP #6 and #8 exhibited a low frequency (~20%) across all samples, SNP #5 was unique to four specific samples. SNP #5 corresponds to the *SF3B1* K700E mutation (Chr2:197,402,110 T → C), a mutation frequently observed at a subclonal level in CLL patients (Wan and Wu 2013; Landau et al. 2015, 2017). The K700E mutation can interrupt the recruitment of *SF3B1* to the correct 3' end branch site and consequently result in alternative splicing (Zhang et al. 2019). We identified the *SF3B1* K700E mutation in CLL3 and CLL26 in both screening (S) and venetoclax-relapsed (R) samples (Supplemental Fig. S8A). This mutation was also confirmed by the WES data from these samples (Thijssen et al. 2022). In scRaCH-seq, the K700E mutation was consistently observed with an overall frequency of 45.0% across the four samples, encompassing 87,674 UMI counts at the location of the *SF3B1*

K700E mutations and 48,224 UMI counts containing the reference base (Thymine) (Fig. 4B). Although SNP #1 and #3 were specific to four samples and occurred at a high frequency, the overall UMI coverage for these altered transcripts was low (Fig. 4A,B). A comparison of scRaCH-seq efficiency in capturing the *SF3B1* K700E mutation with whole transcriptome short-read sequencing (scRNA-seq) and long-read sequencing (scFLT-seq) revealed that scRaCH-seq significantly increased the capture of cells carrying the mutation and enriched for transcripts (Fig. 4C). scRaCH-seq obtains a 14-fold enrichment of reads for *SF3B1* K700E compared to unbiased scFLT-seq, while ~168,000 cells were sequenced versus 1300 cells.

Subsequently, we isolated cells harboring *SF3B1* K700E mutant reads from the scRaCH-seq data and visualized their distribution on the UMAP layout, which contained all patient sample cells (Fig. 5A). Most cells with the mutant reads clustered within the CLL cell group, consistent with the findings from WES. However, a small number of cells with mutant reads were detected within the non-CLL clusters, including the B cell cluster from a HD, T cell cluster, and monocyte cluster (Fig. 5A; Supplemental Fig. S8B). Given that WES established the absence of *SF3B1* mutations in non-CLL cells, we investigated whether these non-CLL cells with *SF3B1* mutant reads might be attributed to false positives induced by doublets. Comparative analysis of UMI counts and gene counts revealed that non-CLL cells with *SF3B1* mutant reads exhibited similar values to CLL cells with *SF3B1* mutants (Fig. 5B). Moreover, expression of multiple lineage markers within the non-CLL cells with *SF3B1* mutant reads was not observed, suggesting that these cells were not doublets (Fig. 5B). In the *SF3B1* wild-type samples confirmed by WES, we identified altered reads with a read fraction of <1% (Fig. 5C), indicative of reads containing sequencing errors (Sereika et al. 2022). To mitigate these false positives in both wild-type samples and non-CLL clusters, we established a threshold based on the abundance of *SF3B1* mutant transcripts detected per cell. This resulted in the exclusion of 80.7% of cells with *SF3B1* mutant transcripts in wild-type samples (Fig. 5C). Furthermore, by raising the threshold to more than 2 *SF3B1* mutant transcripts, 93.4% of false positives in wild-type samples were successfully eliminated (Fig. 5C). Consistent with false positives observed in wild-type samples, most *SF3B1* mutant cells in non-CLL clusters exhibited low counts of altered reads (Fig. 5D). Applying the threshold of more than 2 mutant reads per cell for the identification of a true positive mutant *SF3B1* cell resulted in the removal of most false positives in non-CLL clusters (Fig. 5E). Employing the threshold of more than 2 mutant transcripts based on abundance was then established as a standard quality control step to eliminate false positives during mutation calling. The transcript with altered *SF3B1* #1 was observed in matched samples from CLL3 and CLL5 (Supplemental Fig. S8C). This alteration was observed in both CLL clusters and non-CLL clusters in the UMAP (Supplemental Fig. S8D). These observations suggest that the C-to-G alteration in the *SF3B1* 3' UTR is likely an SNP present at a baseline level in specific patient samples. Notable, even with the threshold in place, we identified SNP #8, a C → T alteration at Chr2:197,421,097, in all samples and across all cell types (Supplemental Fig. S8E,F).

### Detecting the 6 bp deletion in *SF3B1* among CLL cells

In addition to the *SF3B1* K700E point mutation, WES also confirmed the presence of a 6 bp deletion (6 bp-del) at Chr2:197,402,104:197,402,109, resulting in an *SF3B1* KVR700\*\*R

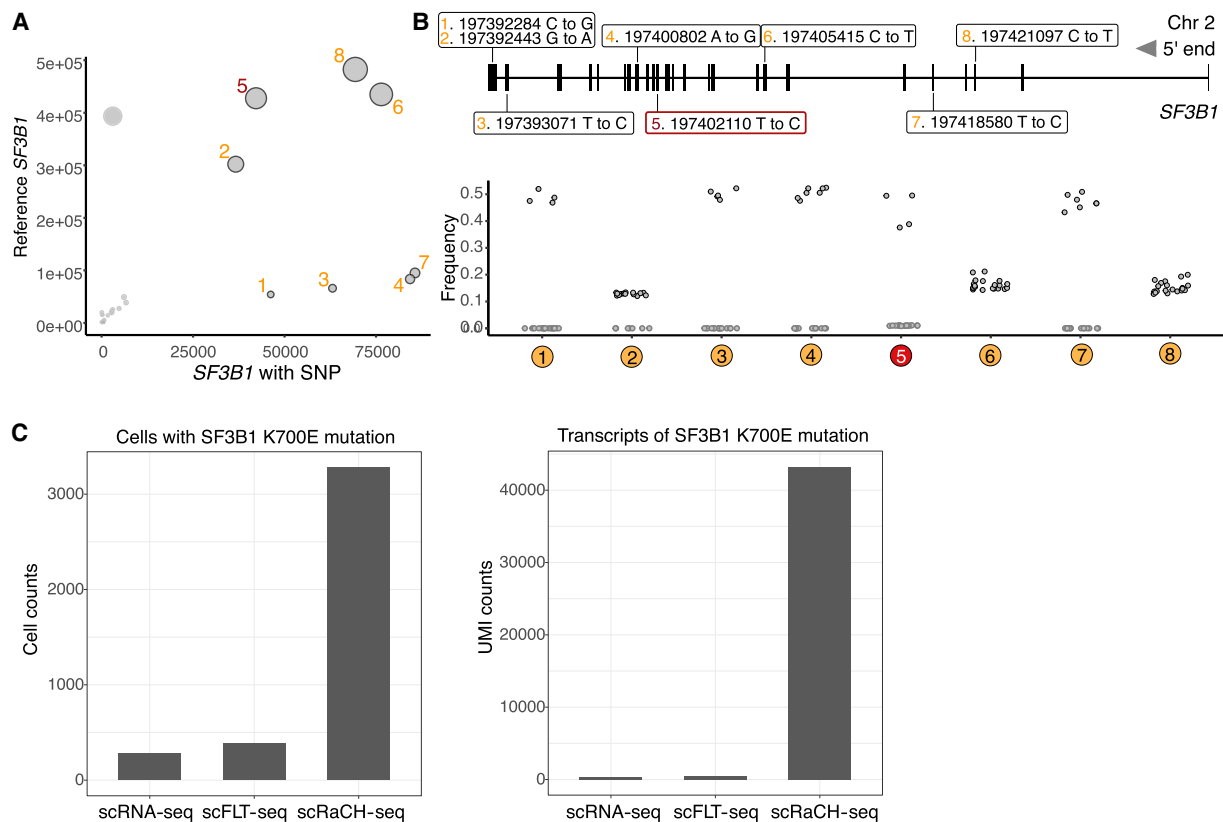


**Figure 4.** Mutation calling with scRaCH-seq and *FLAMES*. (A) Dot plot showing the *SF3B1* point mutations identified using *FLAMES* (left panel). After consolidating reads with UMIs, the reads from all the samples were aligned to the GRCh38 reference genome. The size of each dot in the plot corresponds to the proportion of altered transcripts. (B) A graphical representation highlights the precise locations of these high-frequency (>10%) alterations within the *SF3B1* gene. The bottom graph shows the frequency of altered *SF3B1* transcripts in each sample. (C) Bar plots showing the cells with a *SF3B1* K700E mutation (left panel) or transcripts (UMIs) with *SF3B1* K700E mutation (right panel) detected by short-read scRNA-seq, long-read scFLT-seq, or long-read scRaCH-seq.

mutation in CLL17 at a subclonal level (Thijssen et al. 2022). The original *FLAMES* pipeline was only designed to identify point mutations, so to address this limitation, we developed a supplementary script dedicated to detect the specific deletion directly in the FASTQ files of all samples. To minimize potential false positives, we applied the same criterion as we did for point mutation calling, necessitating at least two transcripts with the deletion per cell across all samples. Notably, cells with the 6 bp deletion were exclusively observed in sample CLL17-R (Fig. 6A), with a predominant clustering within the CLL group (Fig. 6B), aligning with WES findings and underscoring the reliability of the deletion counting method. Subsequently, single-cell differential gene expression analysis was performed to identify gene expression changes between CLL cells with the *SF3B1* deletion and wild-type cells across all venetoclax-relapsed (R) samples. The analysis revealed a total of 377 differentially expressed genes (DEGs) with a  $|\log_2$  fold change (FC)| > 0.5 and adjusted  $P$ -value < 0.05. Among these, 152 genes showed significant upregulation, while 225 genes were downregulated in CLL cells with the KVR700\*\*R mutation (Fig. 6C). Similarly, we identified 147 DEGs (fold discovery rate [FDR] < 0.05) between K700E mutant and wild-type CLL cells, comprising 28 upregulated genes and 119 downregulated genes in *SF3B1* K700E CLL cells (Supplemental Fig. S9A). Given the subclonal nature of the *SF3B1* KVR700\*\*R mutation in CLL17, DE analysis between mutant and wild-type *SF3B1* CLL cells of CLL17 was also conducted. We did not observe any DEGs

(Fig. 6D), implying that the identified DEGs between cells carrying the *SF3B1* 6 bp deletion and wild-type cells are likely relapsed patient-specific rather than mutation-driven.

### Altered splicing in CLL cells with *SF3B1* mutations

It has been reported that the inhibition of RNA splicing can enhance the sensitivity of venetoclax in a mouse model bearing AML (Wang et al. 2023). Therefore, the question remains if *SF3B1* mutation and downstream altered splicing events can contribute to venetoclax resistance in patients with CLL. The current scRaCH-seq probe panel was designed for two target genes to detect isoform usage and mutation calling. However, scFLT-seq from the same samples offers a broader overview of all genes at the transcript level, albeit with lower read coverage per gene (Thijssen et al. 2022). Interrogating the single-cell full-length transcriptomic data showed altered splicing in the CLL cells with *SF3B1* mutation including altered 3' splicing of the *TPT1* gene as an example (Supplemental Fig. S10A,B). This is coherent with previous reports (Tang et al. 2020; Cortés-López et al. 2023); however, we found no evidence of altered splicing transcripts specific to the relapsed *SF3B1*-mutated samples (Supplemental Fig. S10C). Furthermore, no altered splicing of the *BCL2* family genes was observed in *SF3B1*-mutated CLL cells. This finding, in conjunction with the shared enriched pathways uncovered by scRNA-seq data

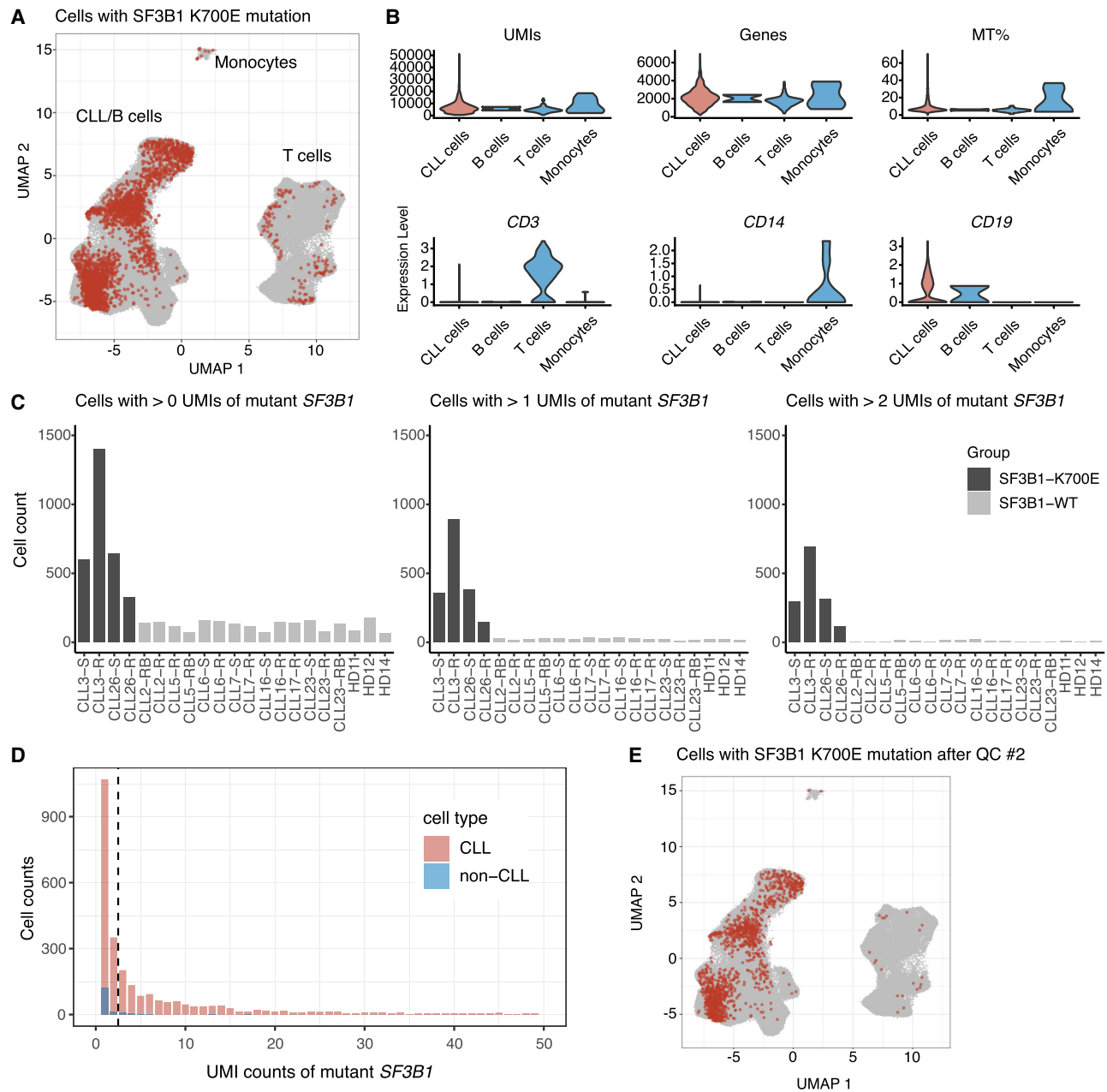


**Figure 5.** The SF3B1 K700E mutation is detected by scRaCH-seq. (A) UMAP projection of cells carrying the SF3B1 K700E mutation (red). (B) Violin plot showing the UMI counts, gene counts (Features), expression of mitochondria genes (MT%), expression of CD3 (T cell marker), CD14 (monocyte marker), and CD19 (B cell marker) per cell type cluster. (C) Bar plot showing the abundance of mutant transcripts. *Left* plot showing cells per sample with >0 transcripts (UMI) of mutant SF3B1 K700E. *Middle* plot showing cells per sample with >1 transcripts (UMIs) of SF3B1 mutation. *Right* plot showing cells per sample with >2 transcripts (UMIs) of SF3B1 mutation. Samples with confirmed SF3B1 K700E mutation by WES are highlighted in dark gray. (D) Bar plot showing the distribution of the abundance of SF3B1 K700E mutation detected in CLL (pink) and non-CLL (blue) cells. The vertical dashed line indicates the criterion of >2 SF3B1 mutation transcripts. (E) UMAP projection of cells carrying >2 SF3B1 K700E mutation transcripts (red).

(Supplemental Fig. S9B,C), suggests that SF3B1 mutations may not play a significant role in the development of acquired venetoclax resistance in CLL cells.

## Discussion

Cell identity and function could be influenced by the alternative splicing of transcripts which will result in a substantial number

of transcript isoforms. However, a significant portion of alternative transcripts will not be detected through high-throughput sequencing-based single-cell RNA-seq methods due to the short-read length and the inherent bias toward 3' or 5' ends of the transcripts (Joglekar et al. 2023). To address this limitation, we developed scRaCH-seq, demonstrating high specificity and efficiency in capturing targeted long-read transcripts. This method provides an in-depth analysis of transcript usage of genes of interest, adding

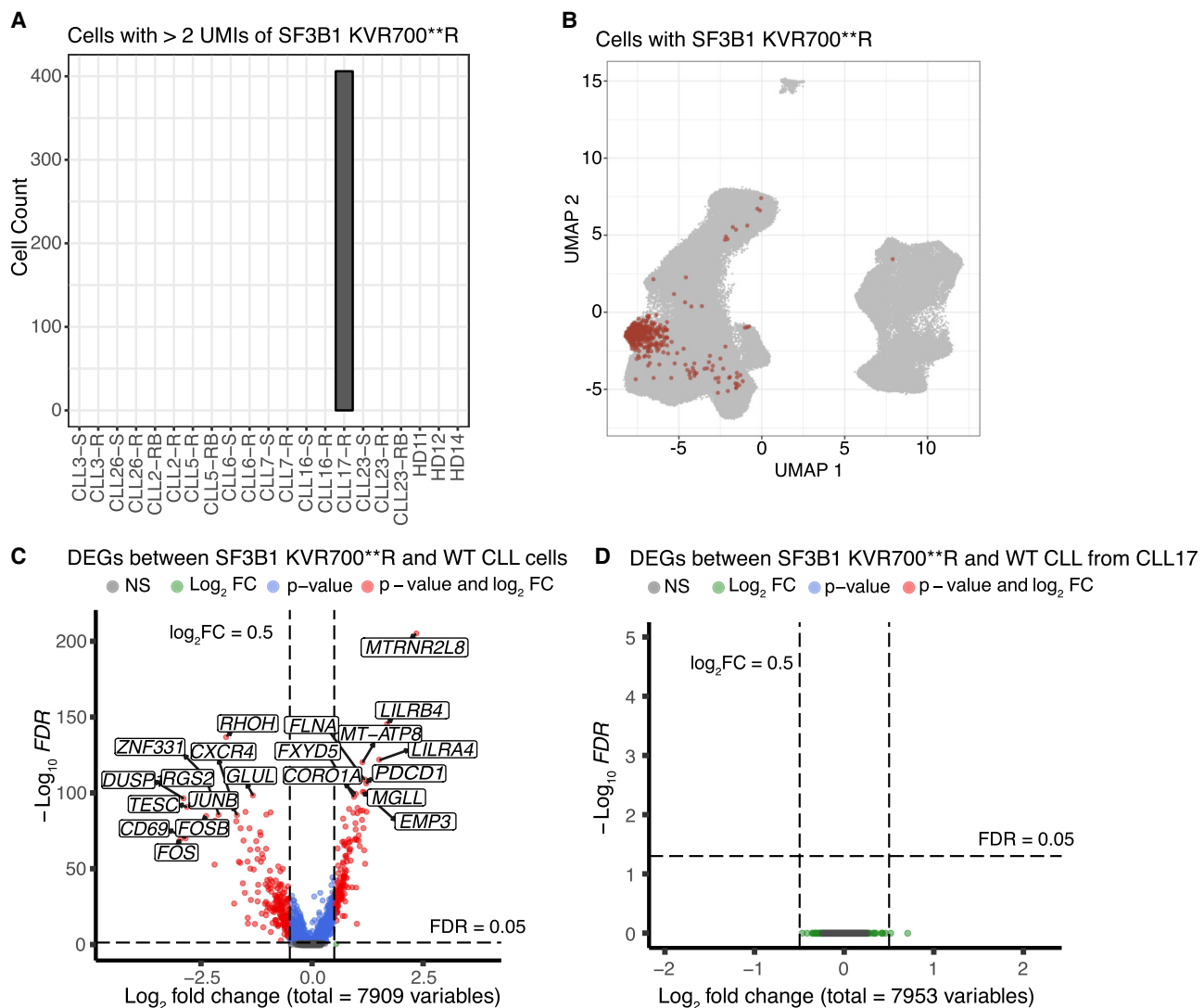


**Figure 6.** The SF3B1 KVR700\*\*R alteration is detected by scRaCH-seq. (A) Bar plot showing the cells with SF3B1 6 bp deletion (Chr 2:197,402,104:197,402,109) across all samples. A criterion of >2 of SF3B1 with 6 bp del transcripts (UMIs) per cell was employed. (B) UMAP projection of cells carrying >2 SF3B1 KVR700\*\*R altered transcripts (red). (C) Volcano plot showing the DEGs (FDR < 0.05) between SF3B1 KVR700\*\*R mutant and wild-type CLL cells from all venetoclax-relapsed CLL samples. (D) Volcano plot showing the DEGs (FDR < 0.05) between SF3B1 KVR700\*\*R mutant and wild-type CLL cells from CLL17.

another layer to the existing single-cell short-read RNA-seq data. Integration of unique barcode primers specific to ONT allowed pooling and efficient sequencing of multiple samples on the Nanopore platform. scRaCH-seq's capability to capture multiple transcripts simultaneously enhances isoform usage detection and facilitates the discovery of transcripts with mutations, providing a valuable tool across diverse research fields. Our study demonstrated the efficient capture of transcripts <5 kb from preindexed and stored cDNA, depending on which genes were targeted. While this study focused on the capture of two genes that are highly expressed, we demonstrated the efficient capture of the transcripts of 17 and 24 genes, with the potential for larger gene sets without the need for primer optimization. Notably, scRaCH-seq demonstrated concordance with scRNA-seq (10x Genomics) in capturing genes, suggesting its reliability in transcriptomic profiling.

We optimized the FLAMES pipeline for scRaCH-seq data by incorporating read integrity checks to eliminate 3' end-truncated reads and setting a quality control threshold of at least two mutant reads to reduce false positives. Additionally, a deletion counting script was created for identifying known deletions. This allowed the detection of the SF3B1 K700E mutation and the 6 bp deletion in SF3B1 in particular samples, both of which were previously confirmed by WES. Meanwhile, the incidence of false positives stemming from sequencing errors was minimal after the filtering based on the abundance of mutant reads detected in CLL cells. While single-cell DNA sequencing, such as Mission Bio Tapestry, provides insight into clonality upon drug resistance (Thompson et al. 2022), it lacks transcriptome profiling per cell. In contrast, scRaCH-seq offers short-read whole transcriptomic data and mutation status if the mRNA of the targeted gene is expressed. By integrating the short-read scRNA-seq data, we observed multiple significant

DEGs between SF3B1 K700E/KVR700\*\*R and wild-type CLL cells. The subclonal nature of SF3B1 KVR700\*\*R in CLL17 allowed us to study the mutation's impact at a single-cell level. No DEGs were observed between SF3B1 KVR700\*\*R and wild-type CLL cells from sample CLL17. However, scFLT-seq demonstrated that the SF3B1 KVR700\*\*R mutation increased the expression of novel isoforms in CLL17. Our single-cell data revealed that the altered gene expression between SF3B1-mutated and wild-type CLL cells was primarily driven by patient specificity. This emphasizes the importance of caution when drawing conclusions based on bulk RNA-seq data comparing wild-type and mutant samples from different patients.

Venetoclax is an effective therapy for CLL patients with the potential to induce long remissions. However, we showed that multiple mechanisms resulting in the deregulation of apoptotic genes could occur at a polyclonal level in venetoclax-relapsed patient samples (Thijssen et al. 2022). Now by incorporating scRaCH-seq, we can add another layer of information and study the effect of an SF3B1 mutation on venetoclax sensitivity. While it was observed that inhibiting RNA splicing could enhance venetoclax sensitivity in AML (Wang et al. 2023), we demonstrated that SF3B1-mutated venetoclax-relapsed CLL cells did not express novel isoforms of the BCL2 family members that could impact venetoclax sensitivity. We observed differential transcript usage of SF3B1 between screening and venetoclax-relapsed samples. SF3B1-211 was found to be specific to a cluster of screening samples but the specific role of this SF3B1 isoform remains unknown. The CLL cells with this SF3B1-211 isoform expressed lower levels of ribosomal genes. These findings suggest a potential connection between the usage of SF3B1-211 transcript and the senescence stage in CLL cells, possibly through its impact on gene transcription activity and protein synthesis.

Lastly, we observed a consistent SF3B1 artifact across all samples in the scRaCH-seq and scFLT-seq data. Comparison of read coverage between scRaCH-seq, scFLT-seq, and bulk RNA-seq data revealed that this artifact resulted from the unexpected binding of the 10x reverse transcriptase primer, rather than being a technical issue with the scRaCH-seq protocol. This unexpected binding of the 10x primers did not impact the results of scRNA-seq since scRNA-seq operates at the gene level, counting all reads aligned to SF3B1. However, it could pose a problem for scFLT-seq and scRaCH-seq, which distinguish reads at the transcript level. Therefore, when identifying novel transcripts in scRaCH-seq or scFLT-seq data, it is advisable to conduct a thorough examination of potential unexpected binding sites of 10x primers within the corresponding gene.

In conclusion, scRaCH-seq provides an innovative strategy for studying long-read transcripts from preindexed cDNA, holding promise for advancing gene expression studies and unraveling complex biological processes. scRaCH-seq can be scaled to the number of target transcripts. We demonstrated a 14-fold read enrichment in capturing a mutation compared to unbiased long-read sequencing, while 21 samples were processed on a single PromethION flow cell versus one sample on a flow cell for unbiased long-read sequencing. Its potential adaptability for PacBio sequencing further extends its utility, with the primary advantage lying in linking transcript usage and mutation status at a single-cell level. The approach is both cost-effective, high-throughput, and flexible, which is achieved by leveraging a wide range of widely used 10x single-cell protocols, making scRaCH-seq applicable for large-scale studies to comprehensively characterize cellular heterogeneity. It holds potential for integration into single-cell spatial

data, representing a powerful advancement in single-cell genomics for understanding cellular heterogeneity in development, disease, and other biological processes.

## Methods

### Samples

The full-length cDNA of 18 peripheral blood samples from CLL patients and three HDs were used (Thijssen et al. 2022). 10x Genomics was performed using the Chromium Next GEM (Gel Bead-In Emulsions) Single Cell V(D)J (v1.1, 10x Genomics PN-1000165) according to the manufacturer's instructions. The indexed full-length surplus cDNA (Thijssen et al. 2022) was stored and used as input for this scRaCH-seq experiment (Fig. 1).

### Probe panel design

Probes were designed to capture the indexed cDNA of target genes. Each probe was 120 bp in length, ensuring robust coverage of the targeted regions. First, a FASTA file was generated for all the isoforms of the genes of interest. The FASTA file containing all Ensembl-annotated exons from all the isoforms was compiled and this was achieved by extracting the corresponding sequences from the human genome GRCh38. This FASTA file served as the foundation for probe design. Next, exon sequences shorter than 120 bp were merged with the preceding and subsequent exons to create concatenations exceeding 120 bp, resulting in an updated FASTA file with all reads over 120 bp. Using the custom FASTA file, a probe panel was generated to cover each base in the input, employing <https://sg.idtdna.com/pages/tools/xgen-hyb-panel-design-tool>. For probe selection, a strategy was implemented to cover every 1000 bp of an exon sequence with a single probe (Supplemental Fig. S1). Probes were selected based on their GC content (GC%) to ensure consistent efficiency during their hybridization with cDNA. The average GC% of the redundant probe panel was used as a baseline. The probe with GC% closest to the average GC% was chosen from the group of probes covering a thousand-base region. For concatenated exons, probes fully covering the entire sequence of the original short exon were selected (Supplemental Fig. S1). Duplicated probes in the selected panel were removed to finalize the probe panel. A prefixed R script (R Core Team 2021) detailing the code for the probe panel design process as well as a step-by-step instruction is available at GitHub (see Data access).

### Single-cell Rapid Capture Hybridization sequencing

#### Amplification of cDNA

The surplus 10x indexed cDNA was amplified to increase the cDNA yield for the hybridization step. To obtain (1.5–2 µg) cDNA, 2–10 ng of cDNA was used as input in 5 × 50 µL reactions. For a 50 µL reaction using 10x Genomics 3' or 5' cDNA, a mixture containing 10 µL 5× PrimeSTAR buffer (Takara R050B), 4 µL dNTP (2.5mM; Takara R050B), 1 µL Partial R1—CTACACGACGCTCTCCGATCT (10 µM), 1 µL TS' PCR Primer IIA—AAGCAGTGGTATCAACGCAGAG (10 µM), cDNA (5–10 ng), nuclease-free water (33 µL-volume cDNA), 1 µL PrimeSTAR GXL DNA Polymerase (Takara R050B) was made. The thermocycler was programmed as follows: 98°C for 30 sec, 9 cycles of 98°C for 10 sec, 65°C for 15 sec and 68°C for 8 min, 1 cycle of 68°C for 10 min. The concentration of the resulting product was assessed, and if it fell below 10 ng/µL, additional cycles were carried out as needed. The pooled amplified cDNA was cleaned up with 0.6× AMPure XP or SPRIselect beads and taken up in 50 µL 5× diluted Elution Buffer (EB; Qiagen) in nuclease-free water (Thermo Fisher Scientific).

We optimized scRaCH-seq so that it can also be applied to 10x Genomics multiome cDNA. A mixture containing 2  $\mu$ L cDNA (2 ng), 25  $\mu$ L 2 $\times$  KAPA HiFi master mix (Roche KK2602), 1  $\mu$ L Partial R1—CTACACGACGCTCTCCGATCT (10  $\mu$ M), 1  $\mu$ L TSOP1—TGGTATCAACGCAGAGTACATGGG (10  $\mu$ M), 21  $\mu$ L EB buffer was made. The thermocycler needs to be programmed as follows: 98°C for 3 min, 8 cycles of 98°C for 15 sec, 64°C for 20 sec and 72°C for 7 min, and 1 cycle of 72°C for 10 min.

### Hybridization

The amplified cDNA sample (1.5–2  $\mu$ g) was dried using a DNA vacuum concentrator (speed vac) together with 1  $\mu$ L of 1000  $\mu$ M IDT Blocking Oligos: Poly(A): TTTTTTTTTTTTTTTTTTTTTTTTTTTT T/3InvdT/, PR1: CTACACGACGCTCTCCGATCT, SO: AAGCAG TGGTATCAACGCAGAGTAC. Subsequently, the dried sample was taken up in the following mixture: 8.5  $\mu$ L of 2 $\times$  Hybridization Buffer, 2.7  $\mu$ L Hybridization Buffer Enhancer (xGen IDT 1080577), and 1.8  $\mu$ L nuclease-free water. The sample was incubated at 95°C for 10 min to denature the cDNA. To this denatured sample, 4  $\mu$ L of custom probe panel was added and incubated at 65°C for 16 h to facilitate probe hybridization with the cDNA.

### Probe pulldown

We used the xGen IDT Lockdown Hybridization and Wash Kit. The sample was added directly to the dried washed beads (100  $\mu$ L of Dynabeads M-270 Streptavidin) and incubated at 65°C for 45 min. Every 10 min the sample and beads were mixed. The captured cDNA was then thoroughly washed, and the bead plus sample mixture was resuspended in 50  $\mu$ L EB.

### Amplification of captured cDNA sample

The captured cDNA with beads was amplified using LA Taq DNA Polymerase Hot-Start (Takara RR042B) in 4  $\times$  50  $\mu$ L reactions. For a 50  $\mu$ L reaction, a mixture containing 5  $\mu$ L 10 $\times$  PrimeSTAR buffer, 4  $\mu$ L dNTP (2.5mM), 1  $\mu$ L FPSfilA: ACTAAAGGCCATTACGGCCT ACACGACGCTCT TCCGATCT (10  $\mu$ M), 1  $\mu$ L RPSfilBr: TTACAG GCCGTAATGGCCAAGCAGTGGTATCAACGCAGAGTA (10  $\mu$ M), 12.5  $\mu$ L cDNA on beads, 26.1  $\mu$ L nuclease-free water, 0.4  $\mu$ L LA Taq DNA Polymerase was made. The thermocycler was programmed as follows: 95°C for 2 min, 12 cycles of 95°C for 20 sec, and 68°C for 10 min, 1 cycle of 72°C for 10 min. After amplification, the cDNA was cleaned up with 0.6 $\times$  AMPure XP or SPRIselect beads and taken up in 30  $\mu$ L EB.

### Nanopore library preparation and sequencing

The ONT SQK-PCB111.24 kit was used to index the samples. Since the cDNA will have the ONT overhang, we started from the “Selecting for full-length transcripts by PCR” step in the protocol with 5  $\mu$ L (1 ng/ $\mu$ L) scRaCH-seq library, 0.75  $\mu$ L Unique Barcode Primer, 6.75  $\mu$ L Nuclease-free water and 12.5  $\mu$ L 2 $\times$  LongAmp Hot Start Taq Master Mix. The thermocycler was programmed as follows: 95°C for 30 sec, 5 cycles of 95°C for 15 sec, 62°C for 15 sec and 65°C for 1 min, and 1 cycle of 65°C for 6 min. After the PCR, the sample was cleaned up with 0.6 $\times$  beads. For the *BTK* and *SF3B1* gene capture, 21 samples were pooled together and sequenced on PromethION R9.4.1 flow cell (Fig. 1).

The scRaCH-seq libraries can also be sequenced on a PromethION R10.4.1 flow cell and using the SQK-NBD114.24 Native Barcoding Kit 24 to index the samples and pool them together. Twelve microliters of 200 fmol of the scRaCH-seq library was combined with 0.1  $\mu$ L Diluted DNA Control Sample (DCS)

and the other protocol components, resulting in a 15  $\mu$ L mixture. This mixture was incubated at 20°C for 10 min and 65°C for 10 min.

## Short-read data analysis

### Data processing

We used Cell Ranger (v5.0.0) and bcl2fastq (v2.19.1) to preprocess our short-read sequencing data. The percentage of mitochondrial gene counts was calculated using the “PercentageFeatureSet” function in Seurat (v4.0.5) (Stuart et al. 2019). This calculation targeted genes starting with the regex pattern “MT-”. For each sample, the “isOutlier” function from Scater (v1.20.0) (McCarthy et al. 2017) was used to identify low-quality cells. These were defined as cells deviating by more than 3 median absolute deviations (MADs) from the median in terms of UMIs (both higher and lower), detected gene numbers (higher and lower), and mitochondrial gene expression (higher). Cells identified as low-quality were then excluded from further analysis. Library size normalization and  $\log_2(x+1)$  transformation were performed using the “NormalizeData” function in Seurat. This step was followed by the identification of highly variable genes (HVGs) using the “FindVariableFeatures” function in Seurat, adhering to default parameters. These HVGs were then scaled and centered with the “ScaleData” function in Seurat.

### UMAP by gene expression

We performed principal component analysis (PCA) by applying the “RunPCA” function in Seurat to scaled HVGs ( $n=2000$ ) with the default parameter settings. To remove the unwanted variability due to batch effects, we applied Harmony (v0.1.0) for batch correction (Korsunsky et al. 2019). For cell clustering analysis, we employed the shared nearest neighbor (SNN) method implemented in Seurat. To construct the SNN graph, we used the “FindNeighbors” function with the first 20 Harmony-corrected PCA embeddings and  $k.param=20$ . For visualization, we generated a UMAP using the “RunUMAP” function with the first 20 Harmony-corrected PCs. To identify cell clusters, we executed the “FindClusters” function on the SNN graph, employing the original Louvain algorithm with default parameters. To identify the doublets, we removed the cluster that exhibited the expression of multiple immune cell lineage markers and high RNA contents. Finally, we applied the same Seurat functions on the filtered data to recluster cells and update the UMAP.

### Single-cell differential expression analysis

To perform single-cell differential expression analysis, we employed the “FindMarkers” function of Seurat, using the parameters configured as `test.use=“MAST”`, `logfc.threshold=0` and `min.pct=0`.

### Pseudo-bulk differential expression analysis

The count matrix for gene expression was aggregated using the “aggregateAcross” function incorporated in Scater. Subsequently, the Likelihood ratio test, implemented in edgeR (v3.34.0) was applied to identify DEGs (Robinson et al. 2010).

### Gene set enrichment analysis

We downloaded the C2 canonical pathways and Hallmark pathway collections using msigdb (v7.5.1) (Liberzon et al. 2015). All genes were then ordered in a decreasing fashion based on their log-fold changes. This ordered list of genes was then used as input for the “GSEA” function in ClusterProfiler (v4.4.4), which was

tested against the gene set collections using default parameters (Wu et al. 2021).

### scRaCH-seq data analysis

We developed a customized *FLAMES* (v1.3.4) pipeline to conduct the scRaCH-seq analysis (Fig. 1). A detailed description of the original *FLAMES* pipeline can be found in the Methods paper that introduces scFLT-seq (Tian et al. 2021).

#### Data preprocessing (STEP 01)

We base called the raw data of nanopore sequencing using the Guppy software (v3.1.5) with the “dna\_r9.4.1\_450bps\_sup\_prom.cfg” configuration, resulting in the generation of FASTQ files. Subsequently, we used the “find\_barcode” function in *FLAMES* to demultiplex the FASTQ files, which was accomplished by cross-referencing the cell barcodes identified in the corresponding scRNA-seq data. We allowed 2 bp of edit distance for the cell barcode matching.

#### Read integrity check (STEP 02)

We added an extra step of reads integrity check to the *FLAMES* pipeline. The demultiplexed reads underwent an examination to confirm the presence of all essential components. These components include a cell barcode, a UMI, a TSO sequence, and a poly (A) tail at the end of the transcript. Users can specify the TSO sequence in the “find\_barcode” function in *FLAMES* and filter reads that are missing the specified TSO sequence.

#### Point mutation calling (STEP 03)

The reads were first aligned to the human genome GRCh38 (downloaded from GENCODE) using the *FLAMES* function “minimap2\_align”. We then used the mutation calling function in *FLAMES* (v0.1) with the default parameters to identify the point mutations, by comparing the pile-up reads against the gene of interest. For *SF3B1*, the gene region Chr2: 197,388,515–197,435,079 from the human genome GRCh38 was selected. For each sample, the positions with alteration frequencies ranging from 10% to 90% were identified as mutations. The allele frequency of identified mutations was then counted and subsequently summarized to generate a mutation count matrix, with the rows corresponding to mutations and the columns named after the cell barcodes.

#### Deletion calling (STEP 03)

We incorporated an additional step specifically to detect multiple base pair deletions in genes of interest. We first aligned the reads which passed the integrity check to the human genome GRCh38, using minimap2 with parameters set as “-ax splice --junc-bonus 1 -k14 --secondary=no --junc-bed” (Li 2018). We then compared the pile-up from the reads to the reference by checking the alignments at the specific chromosomal position. For the *SF3B1* 6 bp deletion previously identified by WES, read alignments were checked at the Chr2:197,402,104–197,402,109 position to identify the presence of the 6 bp deletion. The reads with the multiple base pair deletion were merged by UMIs and subsequently counted for each cell to generate a count matrix, with rows representing the *SF3B1* 6 bp-deletion/WT and column names corresponding to the cell barcodes. We updated *FLAMES* to provide functions for the detection of multiple base pair deletions along with point mutations at both piled-up bulk level (find\_variants) and single-cell level (sc\_mutations) to simplify such analyses.

#### Isoform detection (STEP 04)

We employed the *FLAMES* function “find\_isoform” to summarize the alignment for making isoform assembly. The isoforms that exhibited <10 bp variance in their splicing junctions and <100 bp variance in their start or end sites were merged. Following this, we realigned the reads that passed the integrity check to the isoform assembly to generate the isoform count matrix, with the rows corresponding to isoforms and the columns named after the cell barcodes.

#### Data integration (STEP 05)

We combined the isoform and mutation count matrices with the processed single-cell short-read data to construct a comprehensive multiassay Seurat object, using the “CreateAssayObject” function. The scRaCH-seq data were used to identify cell groups with specific isoforms or mutations, followed by short-read differential expression analysis between these groups.

#### Differential transcript usage analysis

For scRaCH-seq data, we merged the per-cell counts of target gene transcripts by samples to make pseudo-bulk transcript data. We calculated the frequency of different transcripts for our genes of interest *SF3B1* and *BTK*, respectively, and then displayed the top 5 transcripts with the highest frequencies across all samples for both target genes. For scFLT-seq data, cells from patients harboring *SF3B1* mutations/deletions were combined per sample to make pseudo-bulk transcript data for the *SF3B1*-mutated group. Cells of wild-type screening/venetoclax-relapsed/healthy donor samples were merged to construct screening-wt/relapsed-wt/healthy-wt pseudo-bulk transcript data for the *SF3B1*-wild-type group. We then applied the function “diffSpliceDGE” in edgeR to identify the differential transcript usage between groups (*SF3B1*-mutated, *SF3B1*-wt) using pseudo-bulk data as replicates. The scFLT-seq data and WES data involved in this study can be accessed from the European Genome-phenome Archive (EGA; <https://ega-archive.org>) under accession number EGAS00001005815 (Thijssen et al. 2022).

#### Data access

All raw sequencing data generated in this study have been submitted to the European Genome-phenome Archive (EGA; <https://ega-archive.org/>) under accession number EGAD50000000235. The probe panel design code is available at GitHub ([https://github.com/HongkePn/RaCHseq\\_Probe\\_Design](https://github.com/HongkePn/RaCHseq_Probe_Design)) and as Supplemental Code. The complete scRaCH-seq analysis code is available at GitHub ([https://github.com/HongkePn/scRaCHseq\\_data\\_analysis](https://github.com/HongkePn/scRaCHseq_data_analysis)) and as Supplemental Code.

#### Competing interest statement

The authors declare no competing interests.

#### Acknowledgments

We thank Stephen Wilcox, Sarah MacRaild, the WEHI SCORE team, and core facilities (Genomics) for their support. Illustrations were created with BioRender.com. This work was supported by fellowships and grants from the Australian National Health and Medical Research Council: Program Grants 1113133 to D.C.S.H.; Synergy 2011139 to A.H.W., A.W.R., and D.C.S.H.; Fellowship 1156024 to D.C.S.H.; Ideas Grant 2013478 to D.C.S.H. and R.T.; Investigator 2017257 to M.E.R. and 1174902

to A.W.R., the Leukemia & Lymphoma Society of America (Specialized Center of Research [SCOR] grant 7015-18 to A.W.R. and D.C.S.H.), The Australian Research Council (Discovery Project 200102903 to M.E.R.), Leukaemia Foundation (grant 2012526 to R.T.), Victorian Cancer Agency (ECRF21014 fellowship to R.T.), the University of Melbourne (MIRS and MIFRS scholarships to H.P.), the Chan Zuckerberg Initiative DAF (an advised fund of Silicon Valley Community Foundation; grant number 2019-002443 to M.E.R.), and the Amsterdam UMC Fellowship (R.T.). This work was made possible through Victorian State Government Operational Infrastructure Support and the Australian Government NHMRC IRIISS.

**Author contributions:** H.P., D.C.S.H., M.E.R., and R.T. designed the study. A.H.W. and A.W.R. were responsible for patient care and recruited patient samples. H.P., J.S.J., C.C.C., N.S.A., and R.T. acquired the data. H.P., L.T., C.W., Y.Y., N.A., N.M.D., and M.E.R. analyzed and interpreted the data. C.W. updated *FLAMES*. H.P., M.E.R., and R.T. wrote the first version of the manuscript; all authors reviewed the data and contributed to the critical revision of the manuscript.

## References

- Cheng O, Ling MH, Wang C, Wu S, Ritchie ME, Göke J, Amin N, Davidson NM. 2024. Flexiplex: a versatile demultiplexer and search tool for omics data. *Bioinformatics* **40**: btac102. doi:10.1093/bioinformatics/btac102
- Cortés-López M, Chamely P, Hawkins AG, Stanley RF, Swett AD, Ganesan S, Mouhieddine TH, Dai X, Kluegel L, Chen C, et al. 2023. Single-cell multi-omics defines the cell-type-specific impact of splicing aberrations in human hematopoietic clonal outgrowths. *Cell Stem Cell* **30**: 1262–1281.e8. doi:10.1016/j.stem.2023.07.012
- Griffin GK, Booth CAG, Togami K, Chung SS, Ssozi D, Verga JA, Bouyssou JM, Lee YS, Shanmugam V, Hornick JL, et al. 2023. Ultraviolet radiation shapes dendritic cell leukaemia transformation in the skin. *Nature* **618**: 834–841. doi:10.1038/s41586-023-06156-8
- Joglekar A, Foord C, Jarroux J, Pollard S, Tilgner HU. 2023. From words to complete phrases: insight into single-cell isoforms using short and long reads. *Transcription* **14**: 92–104. doi:10.1080/21541264.2023.2213514
- Korsunsky I, Millard N, Fan J, Slowikowski K, Zhang F, Wei K, Baglaenko Y, Brenner M, Loh PR, Raychaudhuri S. 2019. Fast, sensitive and accurate integration of single-cell data with Harmony. *Nat Methods* **16**: 1289–1296. doi:10.1038/s41592-019-0619-0
- Landau DA, Tausch E, Taylor-Weiner AN, Stewart C, Reiter JG, Bahlo J, Kluth S, Bozic I, Lawrence M, Böttcher S, et al. 2015. Mutations driving CLL and their evolution in progression and relapse. *Nature* **526**: 525–530. doi:10.1038/nature15395
- Landau DA, Sun C, Rosebrock D, Herman SEM, Fein J, Sivina M, Underbayev C, Liu D, Hoellenriegel J, Ravichandran S, et al. 2017. The evolutionary landscape of chronic lymphocytic leukemia treated with ibrutinib targeted therapy. *Nat Commun* **8**: 2185. doi:10.1038/s41467-017-02329-y
- Lebrigand K, Magnone V, Barbry P, Waldmann R. 2020. High throughput error corrected Nanopore single cell transcriptome sequencing. *Nat Commun* **11**: 4025. doi:10.1038/s41467-020-17800-6
- Li H. 2018. Minimap2: pairwise alignment for nucleotide sequences. *Bioinformatics* **34**: 3094–3100. doi:10.1093/bioinformatics/bty191
- Liberzon A, Birger C, Thorvaldsdóttir H, Ghandi M, Mesirov JP, Tamayo P. 2015. The Molecular Signatures Database (MSigDB) hallmark gene set collection. *Cell Syst* **1**: 417–425. doi:10.1016/j.cels.2015.12.004
- Liu T, Liu C, Yan M, Zhang L, Zhang J, Xiao M, Li Z, Wei X, Zhang H. 2022. Single cell profiling of primary and paired metastatic lymph node tumors in breast cancer patients. *Nat Commun* **13**: 6823. doi:10.1038/s41467-022-34581-2
- McCarthy DJ, Campbell KR, Lun AT, Wills QF. 2017. Scater: pre-processing, quality control, normalization and visualization of single-cell RNA-seq data in R. *Bioinformatics* **33**: 1179–1186. doi:10.1093/bioinformatics/btw777
- Mustachio LM, Roszik J. 2022. Single-cell sequencing: current applications in precision onco-genomics and cancer therapeutics. *Cancers (Basel)* **14**: 657. doi:10.3390/cancers14030657
- Nagler A, Wu CJ. 2023. The end of the beginning: application of single-cell sequencing to chronic lymphocytic leukemia. *Blood* **141**: 369–379. doi:10.1182/blood.2021014669
- Nam AS, Kim KT, Chaligne R, Izzo F, Ang C, Taylor J, Myers RM, Abu-Zeinah G, Brand R, Omans ND, et al. 2019. Somatic mutations and cell identity linked by genotyping of transcriptomes. *Nature* **571**: 355–360. doi:10.1038/s41586-019-1367-0
- R Core Team. 2021. *R: a language and environment for statistical computing*. R Foundation for Statistical Computing, Vienna. <https://www.R-project.org/>.
- Robinson MD, McCarthy DJ, Smyth GK. 2010. edgeR: a bioconductor package for differential expression analysis of digital gene expression data. *Bioinformatics* **26**: 139–140. doi:10.1093/bioinformatics/btp616
- Ryu KW, Kim D-S, Kraus WL. 2015. New facets in the regulation of gene expression by ADP-ribosylation and poly(ADP-ribose) polymerases. *Chem Rev* **115**: 2453–2481. doi:10.1021/cr5004248
- Sandberg R. 2014. Entering the era of single-cell transcriptomics in biology and medicine. *Nat Methods* **11**: 22–24. doi:10.1038/nmeth.2764
- Sereika M, Kirkegaard RH, Karst SM, Michaelsen TY, Sørensen EA, Wollenberg RD, Albertsen M. 2022. Oxford Nanopore R10.4 long-read sequencing enables the generation of near-finished bacterial genomes from pure cultures and metagenomes without short-read or reference polishing. *Nat Methods* **19**: 823–826. doi:10.1038/s41592-022-01539-7
- Stewart CA, Gay CM, Xi Y, Sivajothi S, Sivakamasundari V, Fujimoto J, Bolisetty M, Hartsfield PM, Balasubramanian V, Chalhazhar MD, et al. 2020. Single-cell analyses reveal increased intratumoral heterogeneity after the onset of therapy resistance in small-cell lung cancer. *Nat Cancer* **1**: 423–436. doi:10.1038/s43018-019-0020-z
- Stoeckius M, Hafemeister C, Stephenson W, Houck-Loomis B, Chattopadhyay PK, Swerdlow H, Satija R, Smibert P. 2017. Simultaneous epitope and transcriptome measurement in single cells. *Nat Methods* **14**: 865–868. doi:10.1038/nmeth.4380
- Stuart T, Butler A, Hoffman P, Hafemeister C, Papalexi E, Mauck WM III, Hao Y, Stoeckius M, Smibert P, Satija R. 2019. Comprehensive integration of single-cell data. *Cell* **177**: 1888–1902.e21. doi:10.1016/j.cell.2019.05.031
- Tang F, Barbacioru C, Wang Y, Nordman E, Lee C, Xu N, Wang X, Bodeau J, Tuch BB, Siddiqui A, et al. 2009. mRNA-seq whole-transcriptome analysis of a single cell. *Nat Methods* **6**: 377–382. doi:10.1038/nmeth.1315
- Tang AD, Soulette CM, van Baren MJ, Hart K, Hrabeta-Robinson E, Wu CJ, Brooks AN. 2020. Full-length transcript characterization of *SF3B1* mutation in chronic lymphocytic leukemia reveals downregulation of retained introns. *Nat Commun* **11**: 1438. doi:10.1038/s41467-020-15171-6
- Thijssen R, Tian L, Anderson MA, Flensburg C, Jarratt A, Garnham AL, Jabbari JS, Peng H, Lew TE, Teh CE, et al. 2022. Single-cell multiomics reveal the scale of multilayered adaptations enabling CLL relapse during venetoclax therapy. *Blood* **140**: 2127–2141. doi:10.1182/blood.2022016040
- Thompson ER, Nguyen T, Kankanige Y, Markham JF, Anderson MA, Handunnetti SM, Thijssen R, Yeh PS, Tam CS, Seymour JF, et al. 2022. Single-cell sequencing demonstrates complex resistance landscape in CLL and MCL treated with BTK and BCL2 inhibitors. *Blood Adv* **6**: 503–508. doi:10.1182/bloodadvances.2021006211
- Tian L, Jabbari JS, Thijssen R, Gouil Q, Amarasinghe SL, Voogd O, Kariyawasam H, Du MRM, Schuster J, Wang C, et al. 2021. Comprehensive characterization of single-cell full-length isoforms in human and mouse with long-read sequencing. *Genome Biol* **22**: 310. doi:10.1186/s13059-021-02525-6
- Tian Y, Li Q, Yang Z, Zhang S, Xu J, Wang Z, Bai H, Duan J, Zheng B, Li W, et al. 2022. Single-cell transcriptomic profiling reveals the tumor heterogeneity of small-cell lung cancer. *Signal Transduct Target Ther* **7**: 346. doi:10.1038/s41392-022-01150-4
- Wan Y, Wu CJ. 2013. *SF3B1* mutations in chronic lymphocytic leukemia. *Blood* **121**: 4627–4634. doi:10.1182/blood-2013-02-427641
- Wang L, Mo S, Li X, He Y, Yang J. 2020. Single-cell RNA-seq reveals the immune escape and drug resistance mechanisms of mantle cell lymphoma. *Cancer Biol Med* **17**: 726–739. doi:10.20892/j.issn.2095-3941.2020.0073
- Wang X, Nissen M, Gracias D, Kusakabe M, Simkin G, Jiang A, Duns G, Sarkozy C, Hilton L, Chavez EA, et al. 2022. Single-cell profiling reveals a memory B cell-like subtype of follicular lymphoma with increased transformation risk. *Nat Commun* **13**: 6772. doi:10.1038/s41467-022-34408-0
- Wang E, Pineda JMB, Kim WJ, Chen S, Bourcier J, Stahl M, Hogg SJ, Bewersdorff JP, Han C, Singer ME, et al. 2023. Modulation of RNA splicing enhances response to BCL2 inhibition in leukemia. *Cancer Cell* **41**: 164–180.e8. doi:10.1016/j.ccell.2022.12.002
- Wu S, Schmitz U. 2023. Single-cell and long-read sequencing to enhance modelling of splicing and cell-fate determination. *Comput Struct Biotechnol J* **21**: 2373–2380. doi:10.1016/j.csbj.2023.03.023
- Wu T, Hu E, Xu S, Chen M, Guo P, Dai Z, Feng T, Zhou L, Tang W, Zhan L, et al. 2021. clusterProfiler 4.0: a universal enrichment tool for

interpreting omics data. *Innovation (Camb)* **2**: 100141. doi:10.1016/j.xinn.2021.100141  
Xu K, Sun S, Yan M, Cui J, Yang Y, Li W, Huang X, Dou L, Chen B, Tang W, et al. 2023. DDX5 and DDX17—multifaceted proteins in the regulation of tumorigenesis and tumor progression. *Front Oncol* **12**: 943032. doi:10.3389/fonc.2022.943032

Zhang J, Ali AM, Lieu YK, Liu Z, Gao J, Rabadan R, Raza A, Mukherjee S, Manley JL. 2019. Disease-causing mutations in *SF3B1* alter splicing by disrupting interaction with SUGP1. *Mol Cell* **76**: 82–95.e7. doi:10.1016/j.molcel.2019.07.017

Received March 13, 2024; accepted in revised form December 10, 2024.